AIP | Applied Physics Letters

A magnesium/amorphous silicon passivating contact for n-type crystalline silicon solar cells

Yimao Wan, Chris Samundsett, Di Yan, Thomas Allen, Jun Peng, Jie Cui, Xinyu Zhang, James Bullock, and Andres Cuevas

Citation: Applied Physics Letters **109**, 113901 (2016); doi: 10.1063/1.4962960
View online: http://dx.doi.org/10.1063/1.4962960
View Table of Contents: http://scitation.aip.org/content/aip/journal/apl/109/11?ver=pdfcov
Published by the AIP Publishing

A magnesium/amorphous silicon passivating contact for *n*-type crystalline silicon solar cells

Yimao Wan,[a] Chris Samundsett, Di Yan, Thomas Allen, Jun Peng, Jie Cui, Xinyu Zhang, James Bullock, and Andres Cuevas
Research School of Engineering, The Australian National University, Canberra ACT 0200, Australia

(Received 25 June 2016; accepted 6 September 2016; published online 15 September 2016)

Among the metals, magnesium has one of the lowest work functions, with a value of 3.7 eV. This makes it very suitable to form an electron-conductive cathode contact for silicon solar cells. We present here the experimental demonstration of an amorphous silicon/magnesium/aluminium (a-Si:H/Mg/Al) passivating contact for silicon solar cells. The conduction properties of a thermally evaporated Mg/Al contact structure on *n*-type crystalline silicon (c-Si) are investigated, achieving a low resistivity Ohmic contact to moderately doped *n*-type c-Si ($\sim 5 \times 10^{15}\,\mathrm{cm}^{-3}$) of $\sim 0.31\,\Omega\,\mathrm{cm}^2$ and $\sim 0.22\,\Omega\,\mathrm{cm}^2$ for samples with and without an amorphous silicon passivating interlayer, respectively. Application of the passivating cathode to the whole rear surface of *n*-type front junction c-Si solar cells leads to a power conversion efficiency of 19% in a proof-of-concept device. The low thermal budget of the cathode formation, its dopant-less nature, and the simplicity of the device structure enabled by the Mg/Al contact open up possibilities in designing and fabricating low-cost silicon solar cells. *Published by AIP Publishing.* [http://dx.doi.org/10.1063/1.4962960]

P-type silicon solar cells are still the workhorse for industrial crystalline silicon (c-Si) solar cell manufacturing. However, as the silicon photovoltaic (PV) industry moves to introduce advanced high-efficiency solar cell concepts, the quality of the base material is becoming more and more important.[1] The high oxygen content in the standard *p*-type Czochralski (Cz) silicon reacts with the boron dopant under illumination and degrades the cell performance, a process known as light-induced degradation (LID).[2,3] *N*-type silicon wafers do not suffer from LID and also feature a higher tolerance to common metal impurities such as Fe, resulting in higher minority carrier diffusion lengths compared to *p*-type counterparts.[2,4] *N*-type wafers therefore have a better material quality, even if made by the Cz method, which allows the full potential of high-efficiency cell designs to be realized.

The use of aluminium to form the anode, or positive, hole-conducting contact, on the rear side of *p*-type crystalline silicon wafers has been a key ingredient of current industrial solar cells. Thanks to the simple, low cost ability to form a highly doped p^+ region upon alloying, which leads to a low contact resistance with an overlying silver contact and a reasonable level of suppression of recombination at the back surface. When Al is directly metallised on *n*-type c-Si (*n*-Si), however, the contact behaves in a rectifying fashion, leading to a high contact resistance. This behaviour is widely attributed to the Fermi-level pinning phenomenon, which leads to a relatively high Schottky barrier height of about 0.65 eV and hinders the flow of electrons out from the *n*-Si wafer.[5,6]

To enable a switch from *p*-type to *n*-type silicon solar cells with the abovementioned concomitant advantages, a tremendous effort has been devoted to overcoming the high Schottky barrier normally found between metals and *n*-type silicon. Historically, an Ohmic contact to *n*-type silicon wafers has been achieved by means of heavy phosphorus doping at the surface of the solar cells via thermal diffusion or plasma deposition (of n^+ a-Si:H). Despite its success in producing record-efficiency silicon solar cells,[7–9] doping creates process complexity and requires either a high temperature, in excess of 800 °C, or high-vacuum plasma deposition using noxious gasses. Recent efforts to overcome such limitations are addressing the challenge of forming electron-selective contacts on *n*-Si wafers without intentional dopants, using materials such as alkali/alkaline metal salts and carbonates (e.g., lithium fluoride,[10–12] magnesium fluoride,[13] and caesium carbonate[14]), transition metal oxides (e.g., titanium oxide[15,16]), and very low work function metals (e.g., calcium[17]). Magnesium (Mg) metal is well known to have a low work function (~3.7 eV) and has been reported to create a relatively low barrier height of 0.35–0.55 eV on *n*-Si.[6,18] Taking advantage of its low work function, Mg has been employed in organic light-emitting devices to enhance electron extraction,[19,20] and also in metal-insulator-semiconductor (MIS) *p*-type silicon solar cells to induce an n^+ inversion layer to replace the conventional phosphorus diffused n^+p junction.[21,22]

Mg has also been investigated to form an Ohmic contact on heavily doped n^+ c-Si. When deposited on an n^+ region with a surface dopant concentration close to $10^{21}\,\mathrm{cm}^{-3}$, a contact resistivity as low as $10^{-7}\ \Omega\ \mathrm{cm}^2$ was achieved.[18,23] Furthermore, an Ohmic contact has been reported between Mg and either intrinsic or phosphorus-doped amorphous silicon (a-Si:H) surfaces, with contact resistivities of $100\ \Omega\ \mathrm{cm}^2$ and $0.5\ \Omega\ \mathrm{cm}^2$, respectively.[24,25] However, the contact resistivity of Mg on intrinsic a-Si:H is far too high for thin film transistors or for solar cells. In addition, neither the effect of the a-Si:H thickness on contact resistivity nor the demonstration of the passivating cathode at the device level was presented.

[a]yimao.wan@anu.edu.au

In this work, we explore the possibility of using Mg to form electron-selective contacts on *n*-type c-Si wafers and solar cells. Note that a capping Al layer is added to suppress the oxidation of Mg in air or during possible final sintering processes. We investigate the conduction properties of a thermally evaporated Mg/Al contact structure on *n*-type c-Si, showing a low contact resistivity ρ_c of $\sim 0.31\,\Omega\,cm^2$ and $\sim 0.22\,\Omega\,cm^2$ to moderately doped *n*-Si ($\sim 5 \times 10^{15}\,cm^{-3}$) for samples with and without an a-Si:H passivating interlayer, respectively. We then apply this passivating electron contact structure to the full rear surface of *n*-type silicon solar cells, achieving a power conversion efficiency of 19%.

Mg layers were thermally evaporated at a rate of 5 Å/s from a 3 N-purity Mg ingot source, with a base pressure of $<2 \times 10^{-6}$ Torr. The a-Si:H interlayers located between the Mg film and the *n*-Si substrate, which were inserted in some cases to suppress the recombination at the c-Si surface, were deposited using a direct plasma enhanced chemical vapour deposition (PECVD) reactor (Oxford PlasmaLab 100) at a temperature set-point of 400 °C, a base pressure of 1.9 Torr, a plasma power of 10 W, a frequency of 13.56 MHz, and a gas flow of 20 sccm. Note that no annealing is required to activate the passivation by a-Si:H used in this work. While the thickness of the metal layer (~10 nm) was determined by the quartz crystal thickness monitor, the thickness of a-Si:H layers was determined by fitting polarized reflectance using the Tauc–Lorentz model,[26] as measured by *ex-situ* spectroscopic ellipsometry (J.A. Woolam M2000 ellipsometer) on the single-side polished c-Si substrate.

The thicknesses of both Mg and a-Si:H layers were also confirmed by the transmission electron micrograph (TEM), as shown in Figure 1. TEM images were acquired from the rear surface of the silicon solar cell that was fabricated as per the procedures to be described later. The cross section of the rear layers was prepared using the focused ion beam (FIB) lift-out technique in a Helios NanoLab 600 DualBeam SEM/FIB system. Final thinning was performed at 5 kV and 16 pA to reduce FIB induced damage. TEM images were obtained using a JEOL 2100 F system operating at 200 kV. Also included in Figure 1 is an energy-dispersive X-ray spectroscopy (EDX) line scan of the local Si, Al, Mg, and O elemental distributions across the interface. Figure 1 seems to indicate some overlap between the Mg and a-Si:H layers, but we ascribe that to an artefact of the TEM/EDX measurement due to a poor TEM/EDX spatial resolution (i.e., ~3 nm). In addition, the possible formation of a sub-oxide species seems to be negligible at the c-Si surface.

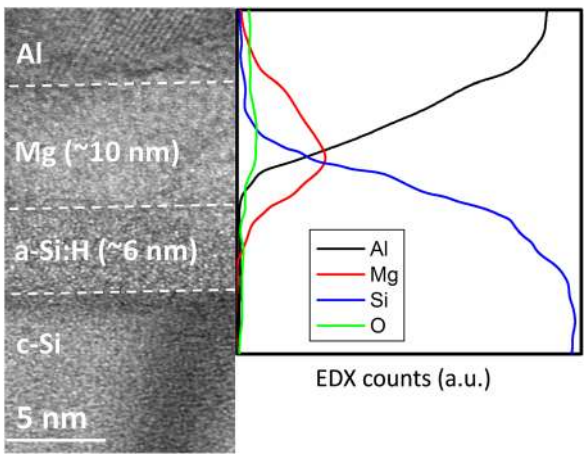

FIG. 1. Transmission electron micrograph (TEM) of the Al/Mg/a-Si:H/*n*-type c-Si structure with an overlying energy-dispersive X-ray spectroscopy (EDX) signal alongside the EDX line scan of the Al, Mg, Si, and O signals (K edges).

A highly selective contact is achieved through a simultaneous reduction in two measurable parameters. The positive selectivity towards majority carriers, that is, the efficient transport of electrons of the Mg/Al contact structure, can be evaluated via its contact resistivity ρ_c. The contact test structures were fabricated on planar Czochralski (Cz) *n*-Si wafers with a resistivity of ~1 Ω cm and a thickness of ~250 μm. Samples were subjected to a dilute HF dip prior to evaporation of the contact structures. An array of circular pads with different diameters was evaporated on the front of the test structures via a shadow mask. A full area Al metal of ~300 nm was evaporated on the rear surface of the contact samples. Current–voltage (*I–V*) measurements were taken at room temperature using a Keithley 2425 source-meter.

Figure 2 shows a series of representative *I–V* measurements of samples with (i) Al metal directly on a-Si:H (~6 nm) passivated *n*-Si (Al/a-Si:H/*n*-Si), (ii) Mg interlayer between Al and a-Si:H passivated *n*-Si (Al/Mg/a-Si:H/*n*-Si), and (iii) Al/Mg directly on *n*-Si (Al/Mg/*n*-Si). Note that the *I–V* measurements of the three groups of samples were performed on the same pad area ($\sim 1.96\,cm^2$) for direct comparison. As we can see in Figure 2, the sample with Al directly on a-Si:H/*n*-Si (i.e., without Mg) exhibits rectifying behavior, similar to the behavior of Al/*n*-Si,[13] preventing an accurate extraction of contact resistivity. In contrast, the insertion of a thin Mg (~10 nm) layer improves dramatically the conductivity of the

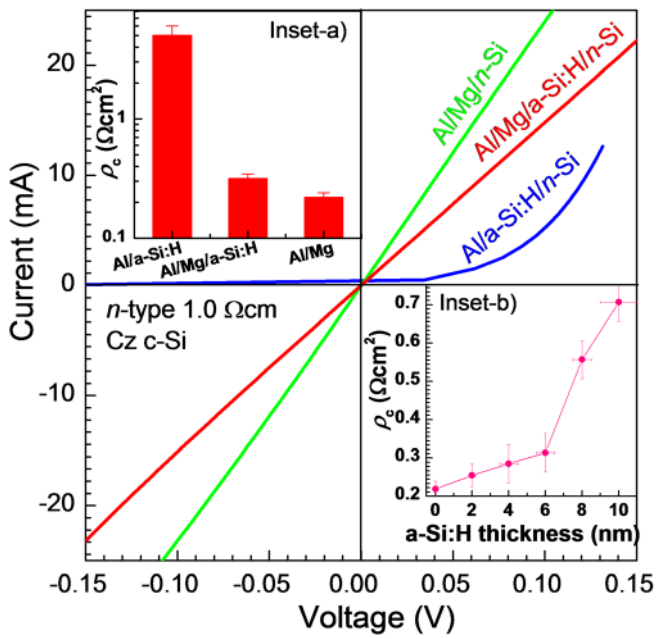

FIG. 2. Representative *I–V* measurements of samples with (i) Al metal directly on a-Si:H (~6 nm) passivated n-Si (Al/a-Si:H/*n*-Si in blue), (ii) Mg interlayer between Al and a-Si:H passivated *n*-Si (Al/Mg/a-Si:H/*n*-Si in red), and (iii) Al/Mg directly on *n*-Si (Al/Mg/*n*-Si in green). The extracted contact resistance ρ_c for the three samples are plotted in inset (a). Inset (b) shows the ρ_c as a function of a-Si:H thickness.

contacts, leading to an Ohmic contact (i.e., linear *I–V* curve) between the Al electrode and the *n*-Si substrate. The extracted contact resistance ρ_c for the structure with Mg is determined to be $\sim 0.22\,\Omega\,cm^2$, which is more than one order of magnitude lower than that without the Mg layer. The higher electron conductivity provided by the Mg/Al contact structure is mainly attributable to the lower work function of Mg, compared to that of Al. It is worth noting that (i) a low work function might only serve as a general guideline for the formation of a good contact by reducing the Schottky barrier height for electron transport and that (ii) surface states still can play a key role in the final height of the metal-semiconductor barrier (Fermi level pinning).

Furthermore, also included in Figure 2 is the ρ_c of the samples with ~6 nm a-Si:H, exhibiting only a slightly higher ρ_c of $\sim 0.31\ \Omega\ cm^2$, as shown in Figure 2 inset-(a). One of the drawbacks of inserting an intrinsic a-Si:H interlayer is that it can introduce additional resistance to current transport through the contact structure. Figure 2 inset-(b) presents the dependence of the measured ρ_c on a-Si:H thickness. It can be seen that ρ_c increases as the a-Si:H thickness increases, exhibiting approximately a factor of 4 increase as the a-Si:H layer increases from 0 to 10 nm. The increase in ρ_c for thicker a-Si:H films is likely due to the bulk resistivity of the a-Si:H, as also revealed in Ref. 13. Preliminary studies indicate that the thickness of the Mg layer has a negligible impact on contact resistivity when it is greater than 2 nm, both for samples with and without an a-Si:H layer. Mg films thinner than 2 nm were difficult to deposit controllably, due to very low melting point of the Mg metal, which caused a fluctuating evaporation rate.

Given that the surface passivation quality by a-Si:H has been shown to saturate when a-Si:H reaches ~6 nm (see Ref. 13) and that a reasonably low ρ_c ($\sim 0.31\,\Omega\,cm^2$) can still be maintained at this thickness, a 6 nm a-Si:H/10 nm Mg/300 nm Al stack was employed for the proof-of-concept cell design. Figure 3(a) depicts the schematic structure of such an *n*-type front-junction silicon solar cell with a full-area rear a-Si:H/Mg/Al contact. Compared to conventional high-temperature diffused n^+ contacts, an advantage of the full area electron contacts is the removal of (i) the high-temperature phosphorus diffusion; and (ii) the patterning of the rear dielectrics (by photolithography in many labs, and commonly by laser ablation in industry).

Solar cells were fabricated on Cz *n*-type c-Si wafers with a resistivity of $\sim 1.0\,\Omega\,cm$ and a thickness of $\sim 200\,\mu m$. The as-cut (100)-oriented silicon wafers were subjected to an alkaline solution of TMAH, deionized water, isopropyl alcohol (IPA), and dissolved silicon at a temperature of 85 °C for 60 min, forming textured morphologies with an array of random pyramids.[27–31] The resultant final wafer thickness is $\sim 175\,\mu m$. After cleaning all samples by the Radio Corporation of America procedure, full-area boron diffusion with a sheet resistance of $\sim 120\ \Omega/\square$ was then performed in a dedicated clean quartz furnace. The front boron diffused textured surfaces were then passivated with a stack of ~20 nm atomic layer deposited (ALD) alumina (Al_2O_3) and ~65 nm PECVD silicon nitride (SiN_x). The undiffused rear silicon surfaces were then fully coated with the a-Si:H/Mg/Al layers. The front metal grid contact with $10\,\mu m$ width lines and 1.3 mm pitch was patterned via photolithography, followed by thermal evaporation of a Cr (~10 nm)/Pd (~10 nm)/Ag (~100 nm) stack, and finally thickened by Ag electroplating.

The photovoltaic *J–V* behavior was measured under standard one sun conditions (100 mW/cm^2, AM1.5 spectrum, 25 °C) with a 2×2 cm aperture mask using a solar simulator from Sinton Instruments. This simulator was calibrated with a certified Fraunhofer CalLab reference cell. The spectral response and reflectance measurements were taken using a Protoflex Corporation QE measurement system (QE-1400-03) and a PerkinElmer Lambda 1050 UV/VIS/NIR spectrophotometer (with an integrating sphere attachment), respectively.

The *J–V* photovoltaic characteristic curve under one sun standard illumination is plotted in Figure 3(b) for cells with

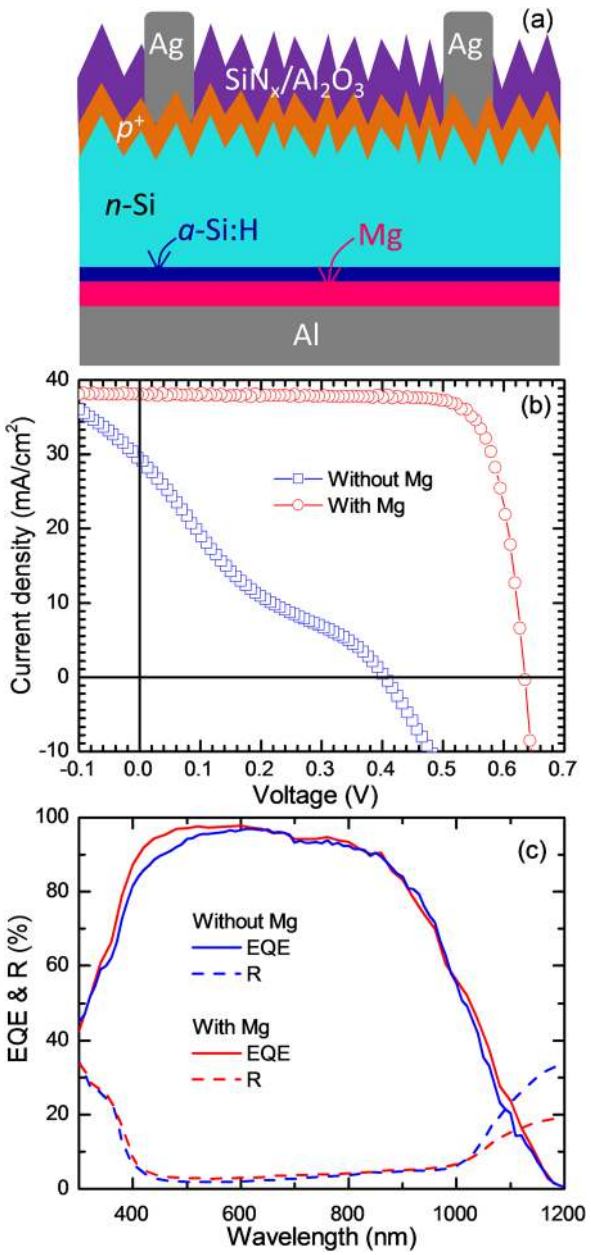

FIG. 3. (a) The schematic structure of an *n*-type front-junction silicon solar cell with a full-area rear a-Si:H/Mg/Al contact. (b) The photovoltaic *J–V* behavior of cells without and with Mg metal interlayer measured under standard one sun conditions. (c) The external quantum efficiencies accompanied the measured reflectance for cells without and with Mg metal interlayer.

TABLE I. Photovoltaic performance of cells without and with Mg metal layers.

	V_{OC} (mV)	J_{SC} (mA/cm^2)	*FF* (%)	η (%)
Without Mg	405.0	29.5	18.2	2.2
With Mg	636.6	38.0	78.4	19.0

and without Mg interlayers. As can be seen, Al directly on the a-Si:H passivated *n*-Si (i.e., without Mg) rear side behaves as a severe Schottky diode, which opposes the photovoltaic effect of the front pn junction, leads to a typical S-shape *J–V* curve, and results in a power conversion efficiency of only 2.2%. Such cell behavior is consistent with the rectifying contact of Al/a-Si:H/*n*-Si presented above. By contrast, the insertion of a Mg layer enhances substantially the cell performance, leading to a conversion efficiency of 19%.

The electrical parameters of the two cells are also summarized in Table I. The reasonable *FF* of the cell with a Mg layer demonstrates a good transport of electrons across the contact structure. Figure 3(c) presents the accompanying spectral response analysis for the two cells. Interestingly, the two cells (i.e., with and without Mg layers) have similar performance in quantum efficiency, despite a significant discrepancy in electrical parameters (i.e., the *J–V* curves). The results imply that, although the cell without Mg layer has similar carrier generation and recombination and slightly higher rear reflectance, it has a very poor electron transport to the electrode due to the rectifying contact at the rear surface. It should be noted that the loss in J_{SC} shown for this cell in Figure 3(b) due to excessive contact resistance does not occur during the quantum efficiency measurement, due to the much lower current levels produced by the monochromatic illumination.

Finally, the V_{OC} of the final device is 636.6 mV, which is significantly lower than the implied V_{OC} measured on the symmetrically a-Si:H-passivated lifetime samples (~710 mV). We ascribe the reduction in V_{OC} to a possible degradation in passivation quality upon thermal evaporation of the Mg/Al metal layers. Due to the high opacity of thick metal layers, together with their high dark conductivity, it is impossible to measure the injection dependent minority carrier lifetime and therefore interface recombination parameter J_{0c} using our photoconductance testing instrument.

We utilize here the photoluminescence (PL) imaging technique (BTimaging LIS-R1) with a 1025 nm short-pass filter to qualitatively evaluate the passivation quality by a-Si:H thin film before and after Mg/Al evaporation, as shown in Figure 4. Note that the PL imaging was performed in an uncalibrated mode and therefore the PL mean counts presented here only give an indication in the relative change in recombination at the silicon surfaces. As we can see, under the same illumination and exposure condition, the PL mean counts of the sample with Mg/Al overlayers are significantly lower (approximately by a factor of five) than those of sample without Mg/Al. The result implies a severe degradation in a-Si:H passivation of the c-Si surface upon evaporating the Mg/Al layers, consequently inducing a significant reduction in the cell's V_{OC}. The root cause for the degradation in surface passivation is still unknown and warrants further investigations.

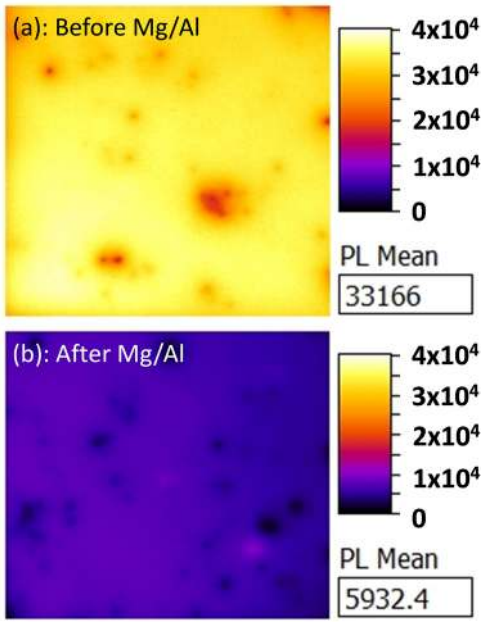

FIG. 4. Photoluminescence (PL) images of a-Si:H passivated samples (a) before and (b) after Mg/Al evaporation using a 1025 nm short-pass filter. Note that the PL imaging was performed in an uncalibrated mode and therefore, under the same illumination and exposure condition, the PL mean counts presented here only give an indication in the relative change in recombination at the silicon surfaces.

In conclusion, we have developed a dopant-free a-Si:H/Mg/Al electron-selective contact deposited at low-temperature. We have investigated the conduction properties of a thermally evaporated Mg/Al contact structure on *n*-type c-Si, demonstrating a sufficiently low contact resistivity of $\rho_c \sim 0.31\,\Omega\,\text{cm}^2$ and $\sim 0.22\,\Omega\,\text{cm}^2$ on moderately doped *n*-Si for samples with and without an amorphous silicon (a-Si:H) passivating interlayer, respectively. Application to the full-area rear surface has enabled a power conversion efficiency of 19%. The low thermal budget of the cathode formation, its dopant-less nature, and the simplicity of the device structure enabled by the Mg/Al contact open up possibilities in designing and fabricating low-cost silicon solar cells.

This work was supported by the Australian Government through the Australian Research Council and the Australian Renewable Energy Agency (ARENA). Some facilities at the Australian National Fabrication Facility at the ANU were used.

[1]S. W. Glunz, J. Benick, D. Biro, M. Bivour, M. Hermle, D. Pysch, M. Rauer, C. Reichel, A. Richter, M. Rudiger, C. Schmiga, D. Suwito, A. Wolf, and R. Preu, paper presented at the 35th IEEE Photovoltaic Specialists Conference (PVSC), 2010.
[2]J. Schmidt and K. Bothe, "Structure and transformation of the metastable boron- and oxygen-related defect center in crystalline silicon," Phys. Rev. B **69**(2), 024107 (2004).
[3]J. Zhao, A. Wang, and M. A. Green, "Performance degradation in CZ(B) cells and improved stability high efficiency PERT and PERL silicon cells on a variety of SEH MCZ(B), FZ(B) and CZ(Ga) substrates," Prog. Photovoltaics: Res. Appl. **8**(5), 549 (2000).
[4]D. Macdonald and L. J. Geerligs, "Recombination activity of interstitial iron and other transition metal point defects in p- and n-type crystalline silicon," Appl. Phys. Lett. **85**(18), 4061 (2004).

[5]D. K. Schroder, *Semiconductor Material and Device Characterization*, 3rd ed. (John Wiley & Sons, Inc., Hoboken, New Jersey, USA, 2006).
[6]S. M. Sze and K. K. Ng, *Physics of Semiconductor Devices* (John Wiley & Sons, 2006).
[7]J. Zhao, "Recent advances of high-efficiency single crystalline silicon solar cells in processing technologies and substrate materials," Sol. Energy Mater. Sol. Cells **82**(1–2), 53 (2004).
[8]S. W. Glunz, F. Feldmann, A. Richter, M. Bivour, C. Reichel, H. Steinkemper, J. Benick, and M. Hermle, "The irresistible charm of a simple current flow pattern-25% with a solar cell featuring a full-area back contact," in 31st European Photovoltaic Solar Energy Conference and Exhibition, 2015.
[9]K. Masuko, M. Shigematsu, T. Hashiguchi, D. Fujishima, M. Kai, N. Yoshimura, T. Yamaguchi, Y. Ichihashi, T. Mishima, N. Matsubara, T. Yamanishi, T. Takahama, M. Taguchi, E. Maruyama, and S. Okamoto, "Achievement of more than 25% conversion efficiency with crystalline silicon heterojunction solar cell," IEEE J. Photovoltaics **4**(6), 1433 (2014).
[10]Y. Zhang, R. Liu, S.-T. Lee, and B. Sun, "The role of a LiF layer on the performance of poly(3,4-ethylenedioxythiophene):poly(styrenesulfonate)/Si organic-inorganic hybrid solar cells," Appl. Phys. Lett. **104**(8), 083514 (2014).
[11]J. Bullock, M. Hettick, J. Geissbühler, A. J. Ong, T. Allen, C. M. Sutter-Fella, T. Chen, H. Ota, E. W. Schaler, S. De Wolf, C. Ballif, A. Cuevas, and A. Javey, "Efficient silicon solar cells with dopant-free asymmetric heterocontacts," Nat. Energy **1**, 15031 (2016).
[12]J. Bullock, P. Zheng, Q. Jeangros, M. Tosun, M. Hettick, C. M. Sutter-Fella, Y. Wan, T. Allen, D. Yan, and D. Macdonald, "Lithium fluoride based electron contacts for high efficiency n-type crystalline silicon solar cells," Adv. Energy Mater. (published online).
[13]Y. Wan, C. Samundsett, J. Bullock, T. Allen, M. Hettick, D. Yan, P. Zheng, X. Zhang, J. Cui, and J. A. McKeon, "Magnesium fluoride electron-selective contacts for crystalline silicon solar cells," ACS Appl. Mater. Interfaces **8**(23), 14671–14677 (2016).
[14]Y. Zhang, W. Cui, Y. Zhu, F. Zu, L. Liao, S.-T. Lee, and B. Sun, "High efficiency hybrid PEDOT:PSS/nanostructured silicon Schottky junction solar cells by doping-free rear contact," Energy Environ. Sci. **8**(1), 297 (2015).
[15]S. Avasthi, W. E. McClain, G. Man, A. Kahn, J. Schwartz, and J. C. Sturm, "Hole-blocking titanium-oxide/silicon heterojunction and its application to photovoltaics," Appl. Phys. Lett. **102**(20), 203901 (2013).
[16]X. Yang, P. Zheng, Q. Bi, and K. Weber, "Silicon heterojunction solar cells with electron selective TiOx contact," Sol. Energy Mater. Sol. Cells **150**, 32 (2016).
[17]T. G. Allen, P. Zheng, B. Vaughan, M. Barr, Y. Wan, C. Samundsett, J. Bullock, and A. Cuevas, paper presented at the IEEE 43rd Photovoltaic Specialists Conference (PVSC), Portland, OR, 2016.
[18]P. L. Janega, J. McCaffrey, D. Landheer, M. Buchanan, M. Denhoff, and D. Mitchel, "Contact resistivity of some magnesium/silicon and magnesium silicide/silicon structures," Appl. Phys. Lett. **53**(21), 2056 (1988).
[19]C. W. Tang and S. A. VanSlyke, "Organic electroluminescent diodes," Appl. Phys. Lett. **51**(12), 913 (1987).
[20]L. S. L. Liao, J. K. Madathil, P. K. Raychaudhuri, and C. W. Tang, Google patents application US 10/062,361 (21 September 2004).
[21]R. B. Godfrey and M. A. Green, "655 mV open-circuit voltage, 17.6% efficient silicon MIS solar cells," Appl. Phys. Lett. **34**(11), 790 (1979).
[22]R. Singh, M. A. Green, and K. Rajkanan, "Review of conductor-insulator-semiconductor (CIS) solar cells," Sol. Cells **3**(2), 95 (1981).
[23]M. Akiya and H. Nakamura, "Low ohmic contact to silicon with a magnesium/aluminum layered metallization," J. Appl. Phys. **59**(5), 1596 (1986).
[24]J. Kanicki, "Contact resistance to undoped and phosphorus-doped hydrogenated amorphous silicon films," Appl. Phys. Lett. **53**(20), 1943 (1988).
[25]H. Matsuura, T. Okuno, H. Okushi, S. Yamasaki, A. Matsuda, N. Hata, H. Oheda, and K. Tanaka, "Ohmic contact properties of magnesium evaporated onto undoped and p-doped a-Si:H," Jpn. J. Appl. Phys., Part 2 **22**(3), L197 (1983).
[26]G. E. Jellison, Jr. and F. A. Modine, "Parameterization of the optical functions of amorphous materials in the interband region," Appl. Phys. Lett. **69**(3), 371 (1996).
[27]M. G. Coleman, W. L. Bailey, C. B. Harris, and I. A. Lesk, U.S. patent 4,137,123 (30 January 1979).
[28]O. Tabata, R. Asahi, H. Funabashi, K. Shimaoka, and S. Sugiyama, "Anisotropic etching of silicon in TMAH solutions," Sens. Actuators, A **34**(1), 51 (1992).
[29]L. M. Landsberger, S. Naseh, M. Kahrizi, and M. Paranjape, "On hillocks generated during anisotropic etching of Si in TMAH," J. Microelectromech. Syst. **5**(2), 106 (1996).
[30]J. S. You, D. Kim, J. Y. Huh, H. J. Park, J. J. Pak, and C. S. Kang, "Experiments on anisotropic etching of Si in TMAH," Sol. Energy Mater. Sol. Cells **66**(1–4), 37 (2001).
[31]P. Papet, O. Nichiporuk, A. Kaminski, Y. Rozier, J. Kraiem, J. F. Lelievre, A. Chaumartin, A. Fave, and M. Lemiti, "Pyramidal texturing of silicon solar cell with TMAH chemical anisotropic etching," Sol. Energy Mater. Sol. Cells **90**(15), 2319 (2006).